

Unusual Baryte-bearing Hybrid Basalt, Bourke-Byrock Area, Northern New South Wales

F.L. SUTHERLAND*, B.J. BARRON†, D.M. COLCHESTER*, A.R. MCKINNON*

Abstract: Drilling near Mount Oxley and Mullagalah in the Bourke-Byrock area, NSW, intersected basaltic breccia pipes. The Mount Oxley basalt is an unusual hybrid rock involving intimate veining and intermingling between a slightly evolved basanite and a strongly evolved, late-stage, baryte-bearing trachyte. The basanite consists of abundant phenocrysts of altered olivine and diopside-augite, and rarer phenocrysts of nepheline, anorthoclase and Ti-rich magnetite, in a groundmass of plagioclase laths and Ti-rich magnetite grains. The trachytic component is dominated by alkali feldspar, largely sanidine, with calcic amphibole (Ti-Mg-rich hastingsite), baryte (with up to 2% Sr in coarser crystals) and secondary carbonates. Olivine-microgabbro and microsyenite xenoliths in the basalt suggest that the cumulates were formed from both the basanitic and trachytic magmas prior to emplacement. Xenoliths of, and xenocrysts from, high pressure ultramafic metamorphic assemblages (spinel harzburgite and spinel websterite) indicate a mantle source for the basanitic magma. Two-pyroxene temperatures based on Wells thermometry suggest these ultramafic assemblages were re-equilibrated under an ambient paleogeotherm between 990–1035°C. Similar basalt appears in the Mullagalah breccia pipe, but lacks the phenocrystic nepheline and the hybrid baryte-bearing trachytic component found in the Mount Oxley basalt. Xenoliths in the Mullagalah breccia include a cumulate-like olivine-bearing diopside-amphibole (K-Ti-rich ferroan pargasite) assemblage. The Mount Oxley and Mullagalah intrusions are not well dated, but were probably formed during Late Mesozoic-Late Cenozoic intraplate basaltic activity that occurred in eastern Australia, from magmas generated at mantle depths exceeding 38 km.

Keywords: Breccia pipe, baryte, basalt, trachyte, xenocrysts, xenoliths

INTRODUCTION

Cenozoic to Mesozoic intraplate basaltic eruptives are a feature in eastern Australia (Johnson 1989, Sutherland 2003). In New South Wales, the most westerly Cenozoic basalts give way to Miocene potassiac, leucite-bearing lavas and minor trachytes, which form a linear, apparently age-progressive trail extending from Byrock, NSW, in the north to Cosgrove, Victoria, in the south (Cundari 1973, Byrnes 1993, Zhang and O'Reilly 1997, Paul et al. 2005, McQueen et al. 2007). Mesozoic intraplate basalts and silicic derivatives also outcrop among the western Cenozoic basalts and are plentiful in the Gunnedah and Dubbo areas (Tadros 1993, Meakin and Morgan 1999). This paper describes an unusual hybrid basaltic intrusion found in this western zone, which was encountered in drill cores near Mount Oxley, east of Bourke (Byrnes 1993). Although this intrusion received petrographic examination, neither nepheline nor baryte were reported. The

significance of these minerals is discussed in this study. Another basaltic diatreme drilled nearby at Mullagalah is also described and is compared with the Mount Oxley intrusion.

The geological setting in the Bourke-Byrock area (Figure 1) forms part of the Palaeozoic Lachlan Orogen, with exposures of folded Ordovician to Devonian sedimentary and volcanic rocks, emplacements of serpentinite and a range of mineralisation (Byrnes 1993). Late Cenozoic leucititic bodies outcrop at Byrock were dated at ~17 Ma (K-Ar dating, Sutherland 1985). Leucititic lavas of similar age outcrop farther south at El Capitan, near Cobar (Ar-Ar dating, McQueen et al. 2007). Minor fresh tholeiitic basalt was also drilled 25 km west of Byrock, but is so far undated (Byrnes 1993). Surficial Cenozoic sedimentary beds, wind blown sands and alluvium from the present Darling, Bogan and Warrego drainages partly obscure bedrock, particularly along the boundary of the Palaeozoic basement rocks and the Mesozoic Surat Basin beds to the north (Figure 1).

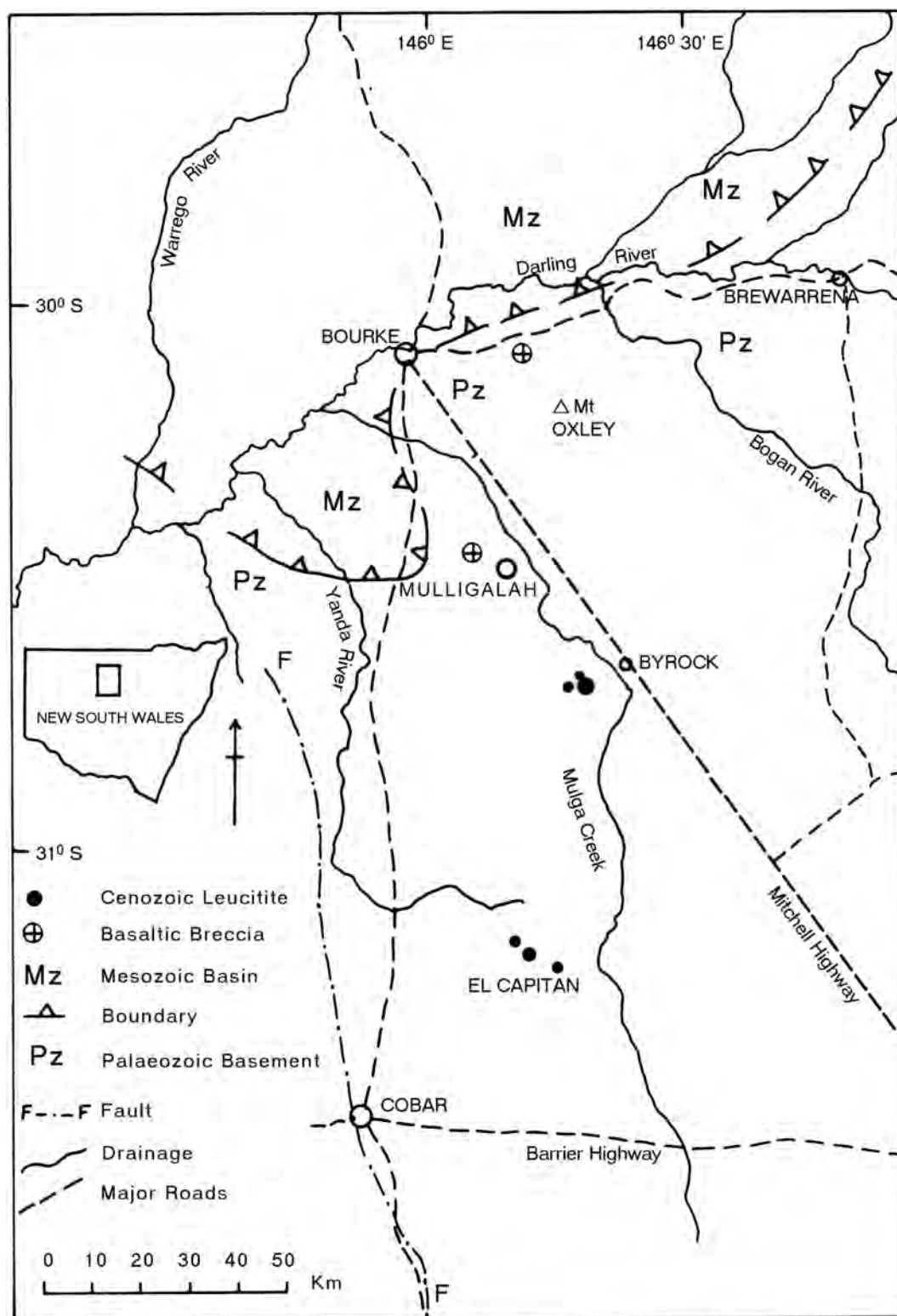


Figure 1. Locality map Bourke-Byrock area, New South Wales, showing locations of the Mt Oxley and Mullagalah basaltic diatremes (drill cores) in relation to the Paleozoic basement rocks, Mesozoic basin boundary, outcrops of Cenozoic leucitites and the main drainages and major roads. Inset shows area within New South Wales.

Samples of the Mount Oxley and Mullagalah basalts and associated intrusive breccias were made available to the authors as fragments, thin sections and polished sections, together with some initial petrographic reports and electron microprobe (EMP) analyses of mineral phases. These materials were donated to the Australian Museum, Sydney, for further study by Dr Ian Plimer, then at North Broken Hill Ltd, and Ian Matthais, CRA Cobar office, in 1983. The Mount Oxley samples (~ 419500 mE, 6671100 mN) came from a hole (T16) drilled by North Broken Hill-Preussag Australia while investigating geochemical prospects and aero-magnetic anomalies at $\sim 146.16^\circ$ E and 30.08° S (Preussag Australia Pty Ltd & North Broken Hill Ltd 1981a,b, North Broken Hill & Preussag Australia Pty Ltd 1982).

The Mullagalah drill core sample (MUI 647) came from a drilling depth of 647 feet within a magnetic anomaly formed by an inclined diatreme west of Mullagalah, at $\sim 146.17^\circ$ E and 30.44° S (North Broken Hill Ltd 1971 a,b). Initial mineral analyses for these company investigations were undertaken by the Geology Department of the University of Melbourne.

Further microscopic studies and mineral analyses were made on the donated samples using facilities at the School of Earth Sciences, Macquarie University and CSIRO Division of Exploration Geoscience, North Ryde, in 1989, and at the School of Natural Sciences, University of Western Sydney, Parramatta, in 2006 to complete the study. Both the Mount Oxley and Mullagalah intrusive basalt breccias contain numerous xenoliths and xenocrysts of the local country rocks and deeper crustal and mantle lithologies which are also described here. The breccias lie southwest of the Bundabulla-Bokhara basalt fields which includes buried alkaline intrusives and rare outcrops (Madden 1999, Jaques 2006 and pers. comm. 2007).

MATERIALS

Mount Oxley

Thin sections cut from the Mount Oxley core are basalt and basalt-intruded breccias (T16, 1-3; S89; 4C3/5). In the breccias, fragments of quartzite and arkose commonly reach up to

9 mm across. The quartz grains in these rocks are highly strained, partly recrystallised and show sutured grain boundaries. Some quartzite fragments show the effects of partial melting where altered brown glassy material is interspersed through the matrix, possibly as minimum melts of K-feldspar. The contact between the breccia and invading basalt is commonly marked by a coarser crystallised feldspathic selvage. The fine grained basalt is porphyritic, and contains rare sub-euhedral nepheline phenocrysts up to 3 mm long (Figure 2). Abundant phenocrysts and glomerocrysts of altered olivine and fresh clinopyroxene, up to 2 mm across, occur with sporadic microphenocrysts of opaque iron oxide and alkali feldspar (Figure 3.1). The olivine is replaced by carbonate and clay. Euhedral clinopyroxenes are sometimes partially resorbed along their margins and exhibit strong core to rim and sector growth zoning. The basalt groundmass ranges from chilled glassy material near its outer contacts with the breccia and grades into a fine grained matrix containing small plagioclase laths and opaque iron oxide grains.

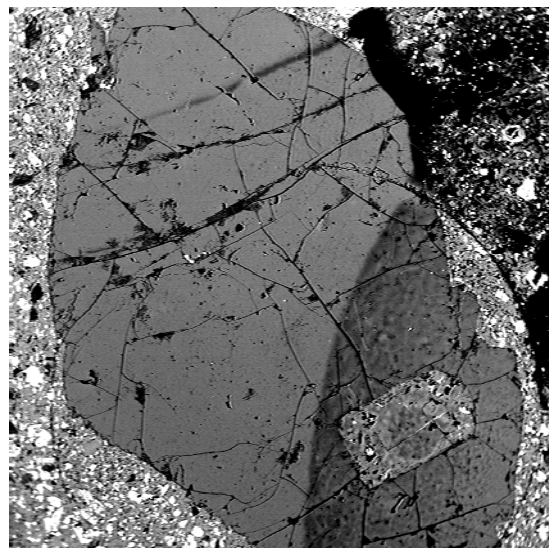
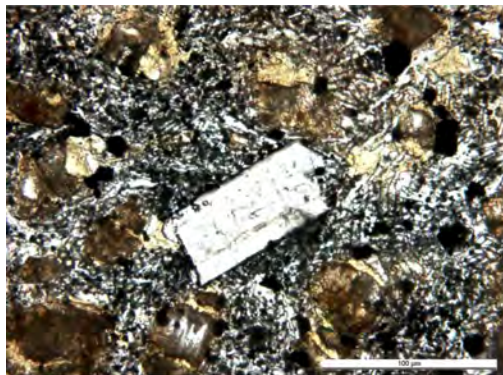


Figure 2. Nepheline ‘phenocryst’ (2.8 mm long, 1.7 mm wide) in basanite, with squarish inclusion of anorthoclase, with reacted margins, within the phenocryst bottom right. Back scattered SEM image. Note bright crystals in the basanite host represent opaque Fe-oxides (Ti-rich magnetite). Photomicrograph: Adam McKinnon.

Trachytic pools, veins and segregations inter-finger with the basalt and represent a late phase of crystallisation (Figure 3.2). Some veins form mosaics of alkali feldspar and in places have broken up and become incorporated into the host basalt. These trachytic veins can reach several centimetres in length and up to a centimetre in width. They grade into amphibole-baryte-carbonate-bearing trachyte that occu-

pies pockets throughout the host basalt, and sometimes invades xenoliths within the host rock. This produces baryte-replacement of pyroxenes in pyroxenites (Figure 4), with baryte surrounding small cores of secondary quartz in some replacements. The last formed veins cut across all other structures in the rocks and represent fracture fillings containing secondary carbonates, clays and iron hydroxides.



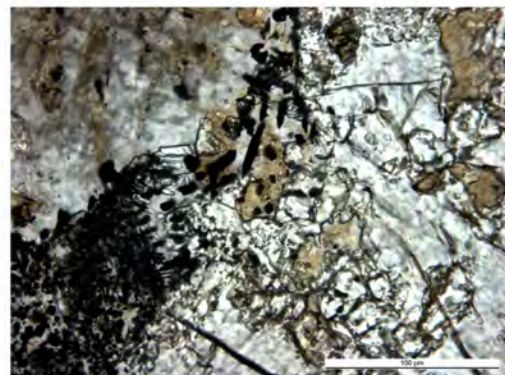
1



2



3



4

Figure 3. Mount Oxley intrusion petrology (T16). 3.1: Anorthoclase microphenocryst (centre) in basanite. Note altered olivine, rare clinopyroxene grains amid plagioclase laths and opaque Fe-oxide grains; 3.2: Pool of baryte-bearing trachyte (lighter coloured, coarser material, centre-right) interacting with basanite host (darker, finer-grained material, left); 3.3: Close up of trachyte pod, showing clinopyroxene prisms (strong relief), scattered amphibole (irregular grayish grains) and rare opaque iron oxide grains in an abundant alkali feldspar-baryte-bearing matrix; 3.4: Reaction zone between baryte-bearing trachyte (lighter material, centre-right) and microgabbro xenolith (grayish material, top left), marked by bladed ilmenite (opaque crystals). Amphibole forms scattered irregular intergrowths. Photomicrographs (PPL): Ian Graham.

Medium to coarse grained xenoliths up to 3 cm across and associated disaggregated xenocrysts are scattered liberally throughout the host basalt. In addition to local crustal materials, there are olivine microgabbro (Figure 5.1) and microsyenite assemblages. These textures suggest that they represent cumulates related to the phenocrystic basalt and its late-stage trachytic component. The microgabbro xenoliths show reaction margins against the trachytic component, which partly replaces olivine (Figure 5.2). Ultramafic metamorphic assemblages among the xenoliths are spinel meta-harzburgite (Figure 5.3), in which olivine is altered to mesh-textured carbonates, talc and clays (Figure 5.4), and spinel meta-websterite. The xenocrysts and composites (derived from the xenolith assemblages) typically show reactions with the host magmas, such as incipient melting and initial crystallisation of secondary minerals (Figure 6.1), feldspathic segregation mantles (Figure 6.2), opaque Fe-oxide reaction rims (Figure 6.3), and strong resorption (Figure 6.4).

Mullagalah

The Mullagalah drill core sample (MU1 647) from a depth of 647 ft (190 m) is an unsorted volcanic breccia (Figure 7.1). It contains volcanic lithic fragments of diverse, but related, basalts

that show various degrees of crystallinity and degradation due to oxidation, as well as abundant xenoliths and xenocrysts of crustal and probable mantle origin. Fragments up to 2 cm across make up 55% of the rock embedded in a pale yellow smectite clay matrix. Basalt forms about 60% of the fragments. The largest of these contains 15% of subhedral altered olivine (up to 1.5 mm across) and sporadic clinopyroxene microphenocrysts (up to 0.2 mm across), some showing hour glass and core to rim zoning (Figure 7.2). The groundmass shows flow banding and strongly chilled broken margins containing up to 40% of flow-aligned prismatic clinopyroxene microlites (Figure 7.3), set in a clay-degraded, in part carbonated and once vesicular volcanic glass. The matrix is charged with minute opaque oxide grains (< 0.02 mm). Olivine phenocrysts are altered to patchy carbonate, talc, and a yellow to brown smectite clay, which also pervades the glassy matrix. Some basaltic fragments contain prominent, euhedral diopside crystals, with simple and knee-shaped twins and partly resorbed margins and interiors. Sparse, altered olivine euhedra reach 1.5 mm. The groundmass contains flow-aligned, wispy plagioclase microlites up to 0.05 mm long, and some cases sections or fragments contain abundant vesicular remnants up to 0.04 mm in yellow brown iron-stained glass.

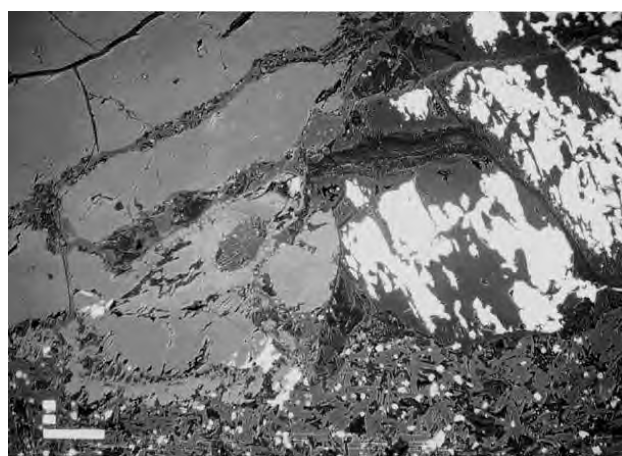
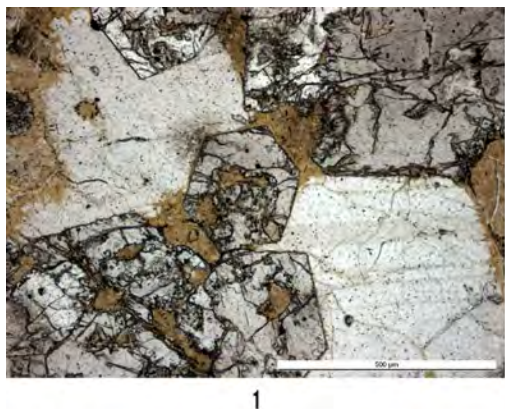


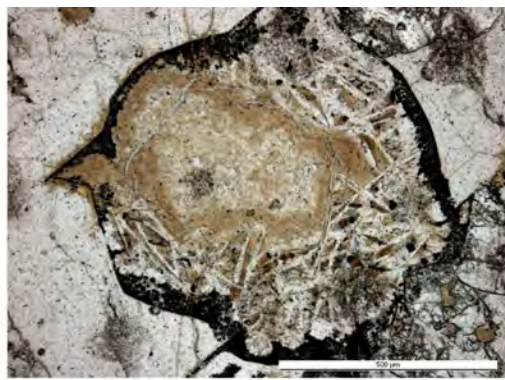
Figure 4. Enstatite-rich meta-websterite, showing invasion of Ba-rich trachyte melt into xenolith. Note replacement of pyroxenes with baryte (bright white patches). The less intense white grains in the host basanite represent Ti-rich magnetite-ulvöspinel grains in the groundmass. Large scale bar = 100 μ m. Back scattered SEM image: K. Kinealy.

The breccia contains a range of xenocrysts (20%) mostly less than 1.5 mm in size. These are cleavage fragments of diopside, pale yellow to orange brown, pleochroic amphibole, yellow-brown Cr-bearing spinel, green spinel; rare opaque Fe-oxides, carbonate-altered olivine, quartz, rare degraded plagioclase and oxidised biotite flakes up to 1 mm long. Some quartz exhibits reactions rims of prismatic diopside. A diopside-amphibole composite 2.5 mm across encloses a small altered olivine grain and may

represents a cognate source for xeno-crystal material (Figure 7.4). Subrounded crustal xenoliths include partly recrystallised microsyenite, foliated feldspathic microbreccia, foliated sandy and silty claystone, deformed and finely recrystallised mircoporphyritic felsic volcanic material, and recrystallised quartzite or vein quartz. The Mullagalah basalts differ from that at Mount Oxley in lacking significant groundmass plagioclase, phenocrystic nepheline or a late-stage baryte-bearing trachytic phase.



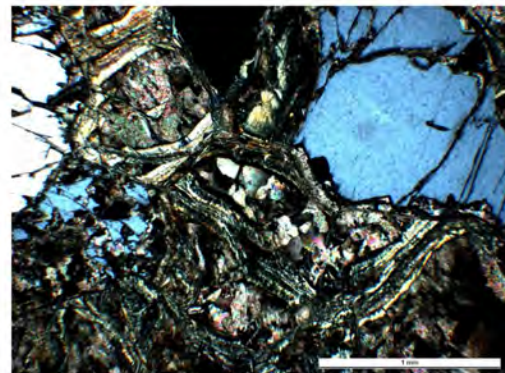
1



2



3



4

Figure 5. Mount Oxley xenolith petrology (T16). 5.1: Cumulate-textured microgabbro, showing euhedral diopside intergrown with large plagioclase crystals, with altered olivine in interstitial grains and inclusions in diopside; 5.2: Altered, reacted olivine grain (centre) in cumulate-textured microgabbro. Note original grain is marked by opaque iron oxide rims, a prominent reaction zone of alkali feldspar laths, intersertal amphibole, partly surrounding a smectitic clay altered core, with coarser trachytic material, bottom right; 5.3: Spinel meta-harzburgite xenolith in basanite host (dark material, left), showing spinel (grey crystal, centre) intergrown with orthopyroxene (lighter crystals, centre top and bottom) and altered olivine (mesh-textured material, centre bottom and right side); 5.4: Meta-harzburgite showing altered olivine, with magnesite replacements (mesh-textured diagonal zone, with mosaic cores), intergrown with orthopyroxene grains (left and right sides). Photomicrographs (PPL): Ian Graham.

ANALYTICAL TECHNIQUES

Because the Mount Oxley basalt is invaded by ubiquitous late-stage baryte-bearing trachytic patches and veins and is riddled with xenocrysts and xenoliths, no bulk chemical analysis of the material was attempted. The mineralogy of the basalts, and a range of xenocryst and xenolith minerals from Mount Oxley and Mullagalalah were investigated using a Leica DMLP polarising microscope. Electron microprobe (EMP) analysis, supplemented with back scattered electron (BSE) imaging confirmed the mineralogy. Because several EMP facilities

were used over a protracted time, the analytical results come from several sources and operators. These include a JEOL probe fitted with wavelength dispersive spectrometers (WDS) at the University of Melbourne (I.R. Plimer and D. Sewell analysts), an automated ETEC probe at Macquarie University, North Ryde (B.J. Barron analyst), a CAMECA system in the Division of Exploration Geoscience, CSIRO, North Ryde (F.L. Sutherland and K. Kinealy analysts) and a JXA super probe with 3 WDS detectors at the School of Natural Sciences, University of Western Sydney, North Parramatta (A.R. McKinnon and F.L. Sutherland analysts).

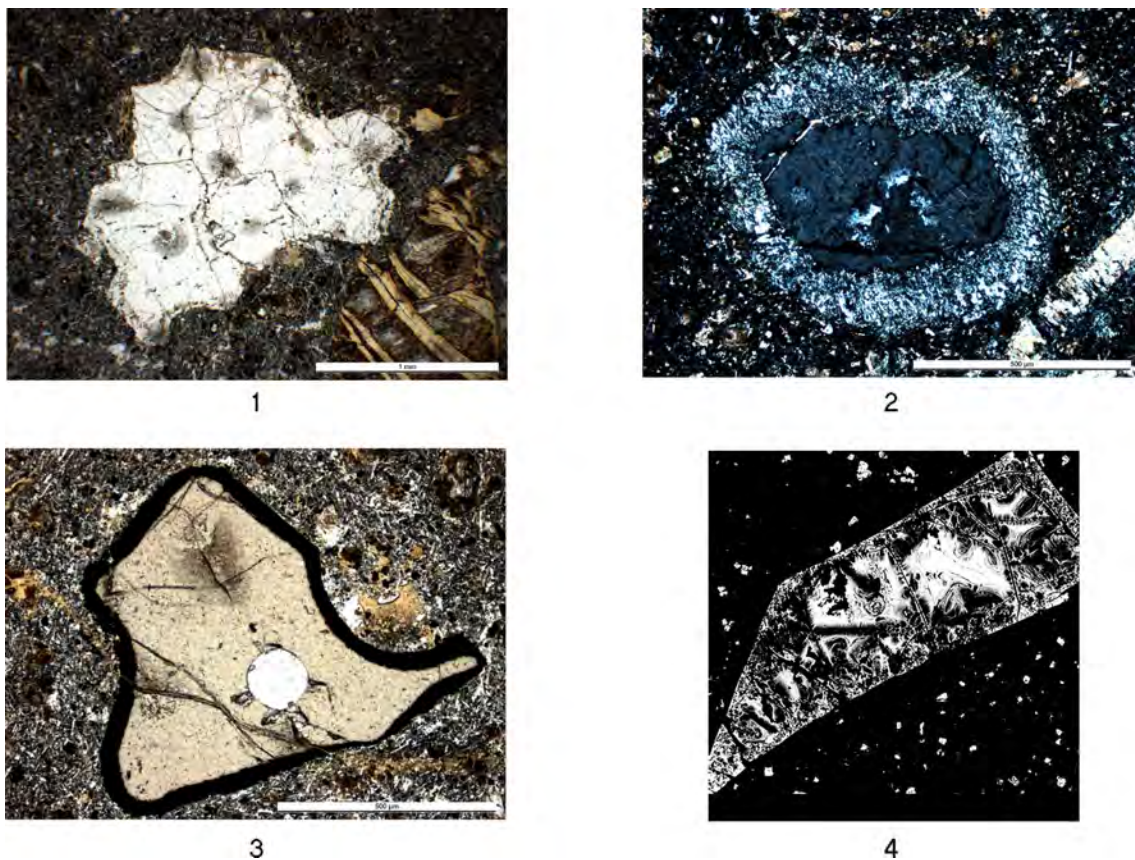


Figure 6. Mount Oxley xenocryst minerals (T16). 6.1: Plagioclase composite xenocryst (centre) in basanite (PPL), showing incipient melting, marked by patchy opaque Fe oxide dustings and invasions along grain boundaries. Note altered olivine phenocryst (bottom right); 6.2: Enstatite xenocryst (dark coloured core) with plagioclase-rich reaction zone (lighter rim) in basanite (XPL); 6.3: Spinel xenocryst (light coloured core) with prominent Fe-oxide reaction zone (opaque rim) in basanite (PPL); 6.4: Resorbed Ti-rich magnetite micro xenocryst (crystal is 1.1 mm long) with more Ti-rich reaction rims, in basanite. Photomicrographs: Ian Graham; Back scattered SEM image: A. McKinnon

Operating procedures and conditions for the EMP analyses mostly utilised a 15 kV acceleration voltage, beam current of 20 nA, Bence-Albee corrections and natural mineral standards. Analytical precision was usually within 1% for elements above 10 wt% as oxides, within \pm 5% at 1–10 wt% oxides and within \pm 10% at < 1 wt% oxides. Because several different instruments provided EMP analyses incorporating a range of variations in base line drift during the runs, as well as potential differences related to surface polish in the samples and operator factors, the results are presented here

as normalised 100% totals. Most results represent anhydrous minerals, while the few hydrous minerals were normalised by assigning a volatile content equivalent to the difference from 100% in the total. The accuracy of the representative analyses listed in Tables 1 to 5 can be judged by the closeness of the calculated cation totals to the theoretical cation total of the unit cell for the analysed mineral. In most cases, cation totals for the anhydrous minerals fell within 0.0–0.5% of the theoretical cation total, while cation totals for the hydrous minerals were usually within 1% of the theoretical totals.

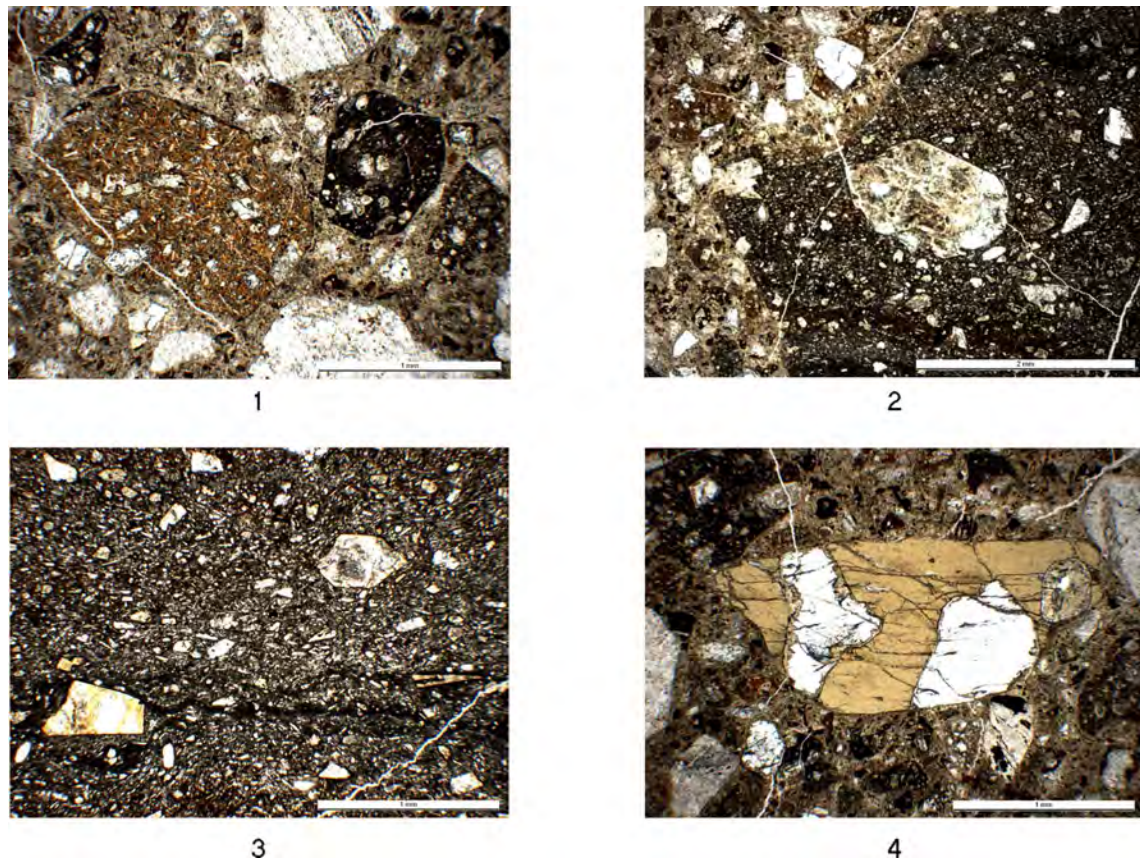


Figure 7. Mullagalagh basalt breccia petrology (MUI 647). 7.1: Basalt fragments in breccia. Note microphenocrysts and plagioclase microlites in ground mass (left fragment) and dark glassy matrix (right fragments), with quartzitic fragments (top and bottom); 7.2: Contact of basalt fragment with breccia (left). Note large altered olivine phenocryst in the basalt (centre); 7.3: Flow-textured basalt fragment. Note alignment of olivine (altered grain, top right), clinopyroxene, microlitic plagioclase crystals and glassy bands; 7.4: Cumulate-like olivine-bearing amphibole (grey zones) and clinopyroxene (light zones) xenolith within breccia. Photomicrographs (PPL): Ian Graham.

End members for the pyroxene group minerals were calculated after the method of Yoder and Tilley (1962) and the computer program of Cebeira (1990). Amphibole compositional names were determined using the computer program of Yavuz (1996). Spinel group end members were calculated from a computer program written by Ross Pogson, Australian Museum. Two-pyroxene temperatures for the co-existing pyroxenes in the ultramafic meta-assemblages used Wells (1977) thermometry which provides the most reliable results for such assemblages (generally within $\pm 50^{\circ}\text{C}$ at temperatures $< 1300^{\circ}\text{C}$; Taylor 1998, Trebaudino and Bruno, 1993). For comparison, Wood and Banno (1973) two-pyroxene temperatures were also calculated and generally yielded results 15–95°C higher.

RESULTS

Representative photomicrographs and mineral analyses of the Mount Oxley and Mullagalah basalt breccias are presented in Figures 2–7 and Tables 1–5.

Mount Oxley Basalt

The phenocryst assemblage is dominated by altered olivine and clinopyroxene (Figure 3.1 and Table 1). The clinopyroxene is zoned Al-rich diopside ($\text{di}_{50-56} \text{hd}_{19-22} \text{tsch}_{20} \text{jd}_{0-8} \text{ac}_{0-5}$), with more calcic, Fe- and Ti-rich rims ($\text{di}_{40} \text{hd}_{29} \text{tsch}_{26} \text{jd}_6$). Sparse opaque oxide phenocrysts belong to a Cr-bearing, Ti-rich magnetite-ulvöspinel series ($\text{usp}_{62} \text{mt}_{17} \text{mf}_8 \text{mc}_7 \text{sp}_7$). Rare large nepheline phenocrysts (Figure 2) are K-bearing ($\text{ne}_{84} \text{ks}_{14}$). They include co-existing zoned alkali feldspar, largely anorthoclase ($\text{ab}_{69} \text{or}_{28} \text{an}_3$), which shows a reaction rim marking the alkali feldspar / nepheline boundary. Alkali feldspar microphenocrysts (Figure 3.1) and twinned, zoned anorthoclase crystals ($\sim \text{ab}_{60-75} \text{or}_{20-32} \text{an}_{5-8}$) may also represent this phenocrystic phase. The groundmass contains plagioclase laths of intermediate composition ($\sim \text{an}_{48-52} \text{ab}_{46-49} \text{or}_{2-3}$), small ulvöspinel grains and rare calcic amphibole grains (alumino-edenite) and variable amounts

of glassy matrix. Overall, the mineralogy represents a porphyritic, evolved ‘nepheline’-bearing basanite.

The invasive late-stage trachytic crystallisations that infiltrate the basalt (Figures 3.2 and 3.3) are dominated by mosaics, tablets and laths of K-rich alkali feldspar, largely sanidine in composition ($\sim \text{or}_{55} \text{ab}_{40} \text{an}_5$). In places the alkali feldspar is inter-grown with clinopyroxene, calcic amphibole (titano-magnesio-hastingsite), interstitial and clustered baryte grains and secondary carbonate fillings. The baryte is Sr-bearing (up to 2%) in coarser crystals (Table 2). Rare isolated green sodic clinopyroxene grains may also belong to this assemblage and classify as hedenbergite, after Yoder and Tilly (1962) ($\text{hd}_{60} \text{di}_{27} \text{jd}_{10} \text{tsch}_2$), or as aegirine-augite under IMA nomenclature (Cebeira 1990). The high jd value favours aegirine-augite over typical hedenergite.

The last-formed veins that cut across all the basalt-trachyte features, incorporated xenoliths and host breccia are dominated by carbonate minerals including magnesite, Al, Fe-rich serpentinitic clay (Wicks and O’Hanley 1988) and nontronitic clay (Güven 1988) (Table 2).

Mount Oxley Xenoliths / Xenocrysts

Xenoliths and xenocrysts in the basalt and breccias represent various lithologies and mineral compositions. Those of interest to the basalt genesis and mantle source include the cumulate-textured magmatic equivalents and high pressure ultramafic metamorphic-textured xenolithic assemblages.

Coarse olivine-clinopyroxene-plagioclase and medium grained olivine-plagioclase cumulates (Figure 4.1) contain similar mineralogy to phenocryst and matrix phases in the basalt and probably represent near-cognate early crystallisations formed prior to basalt eruption. Such crystallisations presumably also provided xenocrysts such as a strongly resorbed ulvöspinel which shows increased Ti contents in the rim zone (Figure 5.4). Other igneous-textured alkali feldspar-rich xenoliths may represent early dismembered K-rich feldspathic cumulates related to the late-stage feldspathic

veins which were introduced into and broken up in the host basalt.

Ultramafic meta-assemblages in the xenoliths include spinel meta-websterites (Figure 4) and spinel meta-harzburgite (Figures 5.3 and 5.4). Two types of meta-websterite differ in the range of Mg contents within the phases (Table 3). One type contains Al-rich enstatite ($\text{en}_{88-89} \text{fs}_{9-10} \text{wo}_{1-2}$), Al-rich augite ($\text{di}_{66-67} \text{tsch}_{16-17} \text{jd}_{6-7} \text{ac}_{6-7} \text{hd}_{3-4}$) and Cr-bearing spinel ($\text{sp}_{74-75} \text{cm}_{13-14} \text{hc}_{8-9} \text{mt}_{2-3} \text{usp}_{0-1}$). Mg numbers for the phases range from 0.90 to 0.72. This type is more magnesian and Cr-rich than in the second type, which contains Al-rich enstatite ($\text{en}_{76-77} \text{fs}_{21-22} \text{wo}_2$), Al-rich augite ($\text{di}_{59-60} \text{hd}_{18-19} \text{tsch}_{12-13} \text{jd}_{8-9} \text{ac}_{1-2}$) and Cr-

bearing spinel ($\text{sp}_{81-82} \text{hc}_{9-10} \text{cm}_{7-8} \text{mt}_{1-2} \text{usp}_{0-1}$). Mg numbers for the phases range from 0.81 to 0.60. Despite the different ranges in Mg numbers, the two types give similar re-equilibrated temperature ranges, based on Wells 2-Pyroxene thermometry ($990^\circ \pm 5^\circ\text{C}$, using Fe^{3+} recalculated T).

The Mg-rich spinel harzburgite (Table 4) contains Al-rich enstatite ($\text{en}_{89} \text{fs}_{9-10} \text{wo}_{1-2}$), Al-rich diopside ($\text{di}_{65-66} \text{tsch}_{14-15} \text{jd}_{9-10} \text{hd}_{5-6} \text{ac}_{4-5}$) and Cr-bearing spinel ($\text{sp}_{81-82} \text{hc}_{9-10} \text{cm}_{6-7} \text{mt}_{1-2} \text{usp}_{0-1}$). Mg numbers for these phases range from 0.91 to 0.78. The Wells 2-Pyroxene T estimates (1005 to 1035°C , Fe^{3+} calculation) are higher than those for the spinel meta-websterite assemblages ($985-1000^\circ\text{C}$).

Mineral	Phenocryst Assemblage, Oxide wt%					
	Cpx	Cpx (core)	Cpx (rim)	Spl	Nep	Alk
SiO_2	48.71	48.90	46.18	0.72	43.39	68.16
TiO_2	0.93	1.65	2.70	20.88	-	-
Al_2O_3	6.92	8.36	7.95	3.07	33.33	17.99
Cr_2O_3	0.83	0.13	0.01	4.77	-	-
Fe_2O_3	2.60	-	-	48.02	-	-
FeO	5.79	6.86	8.95	17.78	0.31	-
MnO	0.18	0.23	0.22	0.65	-	-
MgO	14.27	13.02	11.02	3.35	-	-
CaO	18.94	19.70	22.17	0.34	0.90	0.63
Na_2O	0.71	1.15	0.76	0.20	17.39	8.09
K_2O	-	0.01	0.05	0.02	4.68	4.95
NiO	0.14	-	-	0.17	-	-
Cation Sum	3.999	4.009	4.034	23.912	24.096	19.950
(Oxygens)	6	6	6	32	32	32
Cation Ratios %	Ca 44.0	Ca 45.6	Ca 49.8	Fe 74.4	Na 83.9	Na 69.2
	Mg 42.0	Mg 41.9	Mg 34.5	Ti 19.5	K 14.2	K 27.7
	Fe 14.0	Fe 12.4	Fe 15.7	Mg 6.0	Ca 1.8	Ca 3.0
Name	Augite	Diopside	Diopside	Ulvospinel	Nepheline	Anorthoclase
$\text{Mg}/(\text{Mg}+\text{Fe}^{2+})$	0.815	0.771	0.687	0.254	-	-

Table 1. Representative normalised EMP analyses, phenocryst phases, basanite host (T16, 4C 3/5). Cpx Clinopyroxene, Spl Spinel, Nep Nepheline, Alk Alkali feldspar. Fe_2O_3 and FeO by stoichiometry. Oxygen nos. are based on respective unit cells. Cpx ($\text{di}_{56.1}, \text{tsch}_{20.0}, \text{hd}_{18.5}, \text{ac } 5.1$); Cpx core ($\text{di}_{50.2}, \text{hd}_{21.8}, \text{tsch}_{19.7}, \text{jd}_{8.2}$) and Cpx rim ($\text{di}_{39.9}, \text{hd}_{28.7}, \text{tsch}_{25.6}, \text{jd}_{5.7}$); Spl ($\text{usp}_{61.6}, \text{mt}_{16.7}, \text{mf}_{8.0}, \text{mc}_{7.1}, \text{sp}_{6.8}$); Nep ($\text{ne}_{83.9}, \text{ks}_{14.2}$); Alk ($\text{ab}_{69.2}, \text{or}_{27.7}, \text{an}_{\sim 3.0}$). Dashes indicate concentrations below the level of detection.

Mineral	Late Vein Assemblage (S89), Oxide wt%				Late Alterations (T16)	
	Alk	Amp	Cpx	Bar	Ser	Smc
SiO ₂	64.52	42.02	51.16	-	48.60	44.07
TiO ₂	0.13	3.53	0.40	-	0.12	0.08
Al ₂ O ₃	19.62	14.78	2.28	-	6.69	11.96
Cr ₂ O ₃	0.00	0.47	-	-	0.03	0.05
Fe ₂ O ₃	-	-	4.81	-	-	15.05
FeO	1.04	8.48	13.38	-	13.69	-
MnO	0.00	0.13	0.77	-	0.04	0.01
MgO	0.41	14.45	5.63	-	15.81	1.23
CaO	1.06	10.77	18.69	-	0.72	0.64
Na ₂ O	4.29	2.95	2.88	-	0.24	0.49
K ₂ O	8.87	1.36	0.02	-	0.18	0.21
F2O	-	0.09	-	-	-	-
(H ₂ O)	-	(0.97)	-	-	(13.76)	(26.21)
BaO	-	-	-	63.69	-	-
SrO	-	-	-	1.47	-	-
SO ₃	-	-	-	34.84	-	-
Cation Sum	4.992	16.202	3.976	0.990	5.780	10.217
(Oxygens)	32	23	6	4	9	22
Cation Ratios %	K 54.5	Mg 53.6	Ca 46.3	Ba 96.7	Mg 54.9	Al 51.7
	Na 40.1	Ca 28.7	Fe 34.3	Sr 3.3	Fe 26.7	Fe 41.5
	Ca 5.5	Fe 17.6	Mg 19.4	-	Al 18.4	Mg 6.7
Name	Sanidine	Hastingsite	Hedenbergite	Baryte	Serpentine	Nontronite
Mg/(Mg+Fe ²⁺)	-	0.835	0.429	-	0.673	0.140

Table 2. Representative normalised EMP analyses, baryte-bearing veins, Mt Oxley basanite (S89). Alteration rims, veins, basanite (T16). Alk Alkali Feldspar, Amp Amphibole, Cpx Clinopyroxene, Bar Baryte, Ser Serpentine group, Smc Smectite group. Fe₂O₃ and FeO by stoichiometry. H₂O by difference from 100%. Oxygen nos. from respective unit cells. Alk (or_{54.5}, ab_{40.1}, an_{5.5}); Amp (titano-magnesio-hastingsite); Cpx (hd_{59.7}, di_{27.1}, jd_{10.2}, tsch_{0.2}); Bar (Sr-bearing baryte); Ser (Al-Fe-rich ‘serpentinite’); Smc (nontronite).

Xenocrysts in the basalt such as Mg-Al-rich pyroxenes and spinels show reaction rims (Figures 5.2 and 5.3) and resemble phases in the ultramafic meta-assemblages (Table 4). Compositions are Al-rich enstatite (en_{90-91} fs_{8-9} wo_{1-2}), Al-rich diopside (di_{55-56} tsch_{24-25} hd_{10-11} jd_7 ac_7) and Cr-bearing spinel (sp_{81-82} hc_{9-10} cm_{6-7} mt_{1-2} usp_{0-1}). Mg numbers for these phases range from 0.96–0.71 and match values for these minerals in the ultramafic xenoliths.

Mullagalah Basalt Breccia

The basalt fragments are dominated by phenocrysts of altered olivine and clinopyroxene, in

a fine grained partly glassy groundmass. Only the fresh pyroxene was analysed.

The zoned clinopyroxenes have Al-rich augitic cores (di_{58-59} tsch_{21} hd_{10-11} ac_{8-9} jd_{2-3}) and Al-rich diopsidic outer margins (di_{55-60} tsch_{23-25} hd_{7-10} ac_{9-10}) and Mg numbers range from 0.87 to 0.92 (Table 5). In composition (Ca_{46-47} Mg_{40-47} Fe_{10-13}), they have less Mg and more Fe than clinopyroxene phenocrysts in the Mount Oxley basalt (Ca_{44-50} Mg_{35-42} Fe_{12-16}), which have lower Mg numbers (0.69–0.82). The compositions are also more aluminous (Al_2O_3 8.7–9.0 at%) and sodic (Na_2O 1.3–1.4 at%) than for Mount Oxley clinopyroxene phenocrysts (Al_2O_3 6.9–8.4 wt%; Na_2O 0.7–1.2 wt%).

Mineral	Pyroxenite Xenolith Assemblage (T16), Oxide wt%			Pyroxenite Xenolith Assemblage (S89), Oxide wt%		
	Opx	Cpx	Spl	Opx	Cpx	Spl
SiO_2	54.64	50.98	-	53.39	51.19	-
TiO_2	0.26	0.73	0.34	0.21	0.84	0.21
Al_2O_3	4.89	7.78	53.08	4.30	6.48	60.04
Cr_2O_3	0.52	0.62	12.78	0.16	0.28	7.48
Fe_2O_3	0.00	2.32	0.00	0.00	0.44	0.00
FeO	6.70	1.11	14.53	13.45	5.86	10.63
MnO	0.14	0.11	0.26	0.26	0.18	0.19
MgO	32.08	14.99	18.64	27.14	13.95	21.11
CaO	0.85	19.46	0.01	0.97	19.46	-
Na_2O	0.07	1.89	0.07	0.12	1.32	-
K_2O	0.02	-	0.01	-	-	-
NiO	0.09	0.11	0.29	-	-	0.45
Cation Sum	3.998	3.999	24.171	3.998	4.000	24.134
(Oxygens)	6	6	32	6	6	32
Cation Ratios %	Mg 88.4 Fe 9.9 Ca 1.7	Mg 45.8 Ca 43.7 Fe 10.4	Mg 56.9 Fe 22.4 Cr 20.7	Mg 76.7 Fe 21.3 Ca 2.0	Ca 44.5 Mg 44.4 Fe 11.1	Mg 53.0 Fe 38.2 Cr 8.1
Name	Enstatite	Augite	Spinel	Enstatite	Augite	Spinel
$\text{Mg}/(\text{Mg}+\text{Fe}^{2+})$	0.895	0.707	0.718	0.782	0.809	0.569

Table 3. Representative, normalised EMP analyses. Pyroxenite xenoliths, Mount Oxley basanite. Opx Orthopyroxene, Cpx Clinopyroxene, Spl Spinel. Oxygen nos. are based on respective unit cells. Fe_2O_3 and FeO by stoichiometry. Wells (1977) 2-pyroxene temperatures: T16 (993°C); S89 (988°C). Pyroxenite (T16) phases: Opx ($\text{en}_{88.4}$, $\text{fs}_{9.9}$, $\text{wo}_{1.7}$); Cpx ($\text{di}_{66.9}$, $\text{tsch}_{16.1}$, $\text{jd}_{6.9}$, $\text{ac}_{6.3}$, $\text{hd}_{3.7}$); Spl ($\text{sp}_{74.2}$, $\text{cm}_{13.7}$, $\text{hc}_{8.8}$, $\text{mt}_{2.9}$, $\text{usp}_{0.6}$). Pyroxenite (S89) phases: Opx ($\text{en}_{76.7}$, $\text{fs}_{21.3}$, $\text{wo}_{2.0}$); Cpx ($\text{di}_{59.1}$, $\text{hd}_{18.5}$, $\text{tsch}_{12.6}$, $\text{jd}_{8.2}$, $\text{ac}_{1.2}$); Spl ($\text{sp}_{81.2}$, $\text{hc}_{9.4}$, $\text{cm}_{7.6}$, $\text{mt}_{1.3}$, $\text{usp}_{0.4}$).

Xenoliths in the breccia include a cumulate-like, olivine-bearing clinopyroxene-amphibole composite (Figure 7.4). Clinopyroxene, amphibole and spinel xenocrysts are probably derived from this association. The clinopyroxene is Mg- and Al-rich diopside (\sim di₆₉ tsch₁₂ jd₁₀ hd₇ ac₂; Mg number 0.87–0.94), the spinel is a zoned Cr-bearing member of the spinel-hercynite series (sp_{70–74} hc_{17–21} mt_{4.6} cm₂ usp_{1–2}; Mg number 0.70–0.72) and the amphibole is K-Ti-enriched ferroan pargasite (Table 5). These phases may represent an ultramafic cumulate association, as the clinopyroxene has a higher Mg number (0.93) than for the clinopyroxene phenocrysts in the basalt (0.87–0.92).

Mineral	Xenolith Assemblage			Xenocryst Assemblage		
	Oxide wt%			Oxide wt%		
	Opx	Cpx	Spl	Opx	Cpx	Spl
SiO ₂	54.15	51.39	0.02	54.42	51.02	0.00
TiO ₂	0.13	0.70	0.27	0.14	0.78	0.27
Al ₂ O ₃	5.37	7.76	59.28	4.97	7.74	61.24
Cr ₂ O ₃	0.32	0.71	7.42	0.36	0.49	6.62
Fe ₂ O ₃	0.94	1.68	0.00	0.86	2.55	0.00
FeO	5.72	1.66	10.79	5.53	0.99	9.48
MnO	0.15	0.15	0.41	0.18	0.12	0.14
MgO	31.96	14.90	21.15	32.42	14.78	21.59
CaO	0.90	19.03	-	0.83	19.47	0.03
Na ₂ O	0.14	1.99	-	0.10	1.98	-
K ₂ O	0.01	0.02	0.12	-	0.01	0.01
NiO	0.21	0.04	0.54	0.19	0.08	0.49
BaO	0.02	-	-	-	-	-
Cation Sum	4.000	4.001	23.994	4.001	3.998	24.085
(Oxygens)	6	6	32	6	6	32
Cation Ratios %	Mg 89.0	Mg 50.3	Mg 70.8	Mg 90.7	Mg 50.5	Mg 70.8
	Fe 9.2	Ca 46.2	Fe 17.7	Fe 8.8	Ca 47.6	Fe 17.7
	Ca 1.8	Fe 3.4	Cr 11.5	Ca 1.6	Fe 2.1	Cr 11.5
Name	Enstatite	Diopside	Spinel	Enstatite	Diopside	Spinel
Mg/(Mg+Fe ²⁺)	0.909	0.941	0.784	0.913	0.964	0.708

Table 4. Normalised representative EMP analyses, harzburgite xenolith and xenocryst phases (T16). Opx Orthopyroxene, Cpx Clinopyroxene, Spl Spinel. Oxygen nos. are based on respective unit cells. Fe₂O₃ and FeO by stoichiometry. Xenolith: Opx (en_{89.0}, fs_{9.2}, wo_{1.6}); Cpx (di_{65.7}, tsch_{14.8}, jd_{9.4}, hd_{5.5}, ac_{4.6}); Spl (sp_{81.6}, hc_{8.1}, cm_{7.5}, mt_{2.2}, usp_{0.4}). Xenocrysts: Opx (en_{90.7}, fs_{8.8}, wo_{1.6}); Cpx (di_{55.2}, tsch_{24.1}, hd_{10.5}, jd_{7.0}, ac_{6.9}); Spl (sp_{81.7}, hc_{9.8}, cm_{6.6}, mt_{1.4}, usp_{0.6}). Wells (1977) 2-pyroxene temperature: xenolith (1005°C).

Mineral	Phenocryst assemblage (fresh)			Xenocryst–Xenolith assemblage			
	Oxide wt%			Oxide wt%			
	Cpx	Cpx (core)	Cpx (rim)	Cpx	Spinel (core)	Spinel (rim)	Amp
SiO ₂	47.74	49.11	48.04	52.07	0.01	0.06	39.58
TiO ₂	1.49	1.25	1.37	0.52	0.54	0.62	3.77
Al ₂ O ₃	9.03	8.67	8.87	6.66	59.56	60.03	15.05
Cr ₂ O ₃	0.05		0.03	0.80	1.80	2.02	0.04
Fe ₂ O ₃	3.82	2.98	4.08	0.85	5.28	3.81	12.63
FeO	3.32	3.29	2.20	2.01	13.39	14.71	-
MnO	0.08	0.11	0.09	0.16	0.27	0.22	0.05
MgO	12.39	14.55	13.40	14.85	18.91	18.32	11.89
CaO	20.59	18.58	20.57	20.23	0.02	-	11.30
Na ₂ O	1.38	1.43	1.32	1.73	-	-	2.41
K ₂ O	0.02	0.04	0.01	0.01	0.02	0.01	2.43
BaO	-	-	-	-	-	-	-
NiO	0.08	-	-	0.21	0.17	0.21	0.06
(H ₂ O)	-	-	-	-	-	-	(0.96)
Cation Sum	3.999	3.999	3.971	4.001	24.016	24.008	16.216
(Oxygens)	6	6	6	6	32	32	24
Cation Ratios %	Ca 47.8	Mg 46.5	Ca 47.0	Ca 47.0	Mg 62.9	61.9	Mg 46.6
	Mg 40.0	Ca 42.8	Mg 42.6	Mg 47.0	Fe 33.9	34.4	Ca 31.8
	Fe 12.2	Fe 10.7	Fe 12.2	Fe 5.0	Cr 3.2	3.6	Fe 21.5
Name	Diopside	Augite	Diopside	Diopside	Spinel	Spinel	Pargasite
Mg/(Mg+Fe ²⁺)	0.870	0.888	0.916	0.929	0.716	0.698	1.000

Table 5. Normalised EMP analyses, phenocryst and xenolith phases, Mullagalagh basalt breccia (MUI 647). Cpx Clinopyroxene, Spl Spinel, Amp Amphibole. Oxygen nos. are based on respective unit cells. Fe₂O₃ and FeO by stoichiometry. (H₂O) estimated by difference from 100%. Amphibole (average of 2 analyses). Phenocrysts: Cpx (di_{55.2}, tsch_{24.1}, hd_{10.5}, ac_{10.0}); Cpx core (di_{58.3}, tsch_{21.0}, hd_{10.4}, ac_{8.2}, jd_{2.1}) and Cpx rim (di_{59.7}, tsch_{23.9}, ac_{9.4}, hd_{7.0}). Xenocryst / xenolith: Cpx (di_{68.9}, tsch_{11.9}, jd_{9.9}, hd_{6.6}, ac_{2.3}); Spl core (sp_{73.2}, hc_{17.8}, mt_{6.1}, cm_{1.8}, usp_{1.4}); Spl rim (sp_{70.8}, hc_{20.9}, mt_{4.8}, cm_{2.1}, usp_{1.1}); Amp (potassian, titanian, ferroan pargasite).

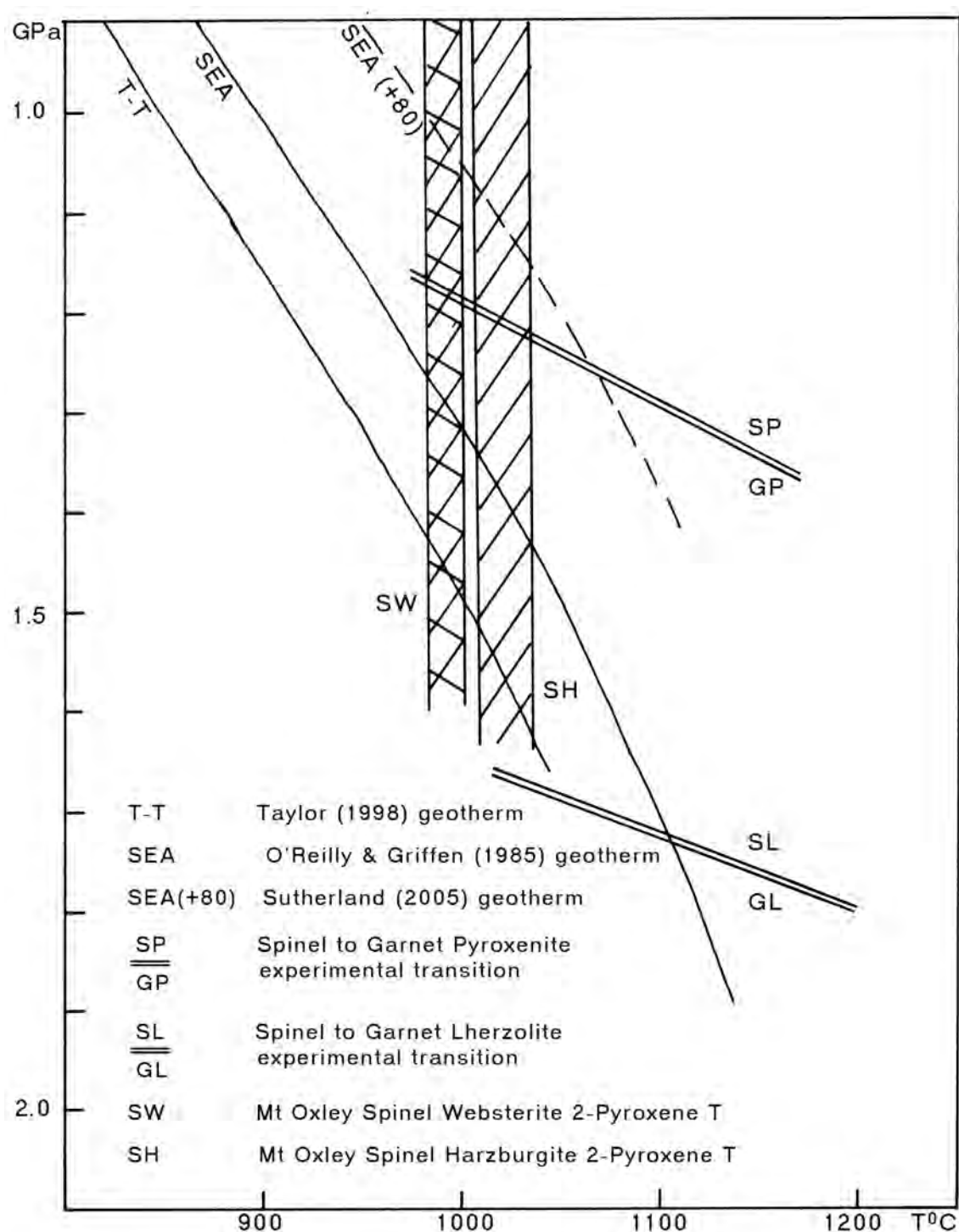


Figure 8. Pressure (GPa)-Temperature (°C) diagram showing relationships of two-pyroxene temperature estimates for Mount Oxley ultramafic xenolith meta-assemblages, with intersections of selected eastern Australian geotherms and experimental mineral assemblage transitions.

DISCUSSION

The porphyritic mafic intrusions described here were related to lamprophyres in some previous reports (Byrnes 1993), and were compared with camptonites and monchiquites. Camptonites contain amphibole together with olivine and clinopyroxene as phenocrysts, while monchquites also contain micas and feldspathoids (Rock 1991). Amphibole is absent from the Mount Oxley phenocrysts, but does occur as a groundmass phase in the hybrid late-stage trachytic crystallisations. This hybrid occurrence is insufficient to justify a camptonite nomenclature and a basaltic terminology is preferred for the mafic host. Amphibole occurs in the Mullagalah basalt, but is xenocrystic and probably derived from amphibole-clinopyroxenite xenoliths. For the ensuing discussion the Mount Oxley and Mullagalah mafic bodies are related to basanitic magmas.

Mount Oxley Basalt Petrogenesis

This basaltic intrusion displays a dual petrogenetic identity. Emplaced as a slightly evolved undersaturated magma, it became closely intermingled with a late-stage barium- and sulfur-bearing, evolved alkaline trachytic melt. The high temperature, high pressure ultramafic xenoliths within the basanite suggest initial evolution took place within the sub-continental mantle lithosphere, although the trachytic material could mark a higher level crustal fractionate. Such mantle-derived lava mingled with evolved felsic lava is rare in eastern Australian intraplate basalts. One example, however, is the meta-lherzolite and granulite xenolith-bearing nepheline hawaiite co-mingled with anorthoclase-bearing trachyte in the 3 Ma Mount St Martin volcanic centre in the Nebo Province, Queensland (Sutherland et al. 1977, Griffin et al. 1987). The hybrid lava there, however, lacked phenocrystic nepheline in the mafic component and baryte in the felsic component, which feature in the Mount Oxley association.

The Mount Oxley basanitic magma began crystallising its phenocrystic phases (olivine and diopside) at mantle depths prior to its

eruption, while some crystallisation probably took place at higher levels to produce cumulate olivine microgabbros, as plagioclase joined the liquidus phases. These gabbros would crystallise at depths shallower than pressures related to the olivine + plagioclase/two pyroxene-spinel transition zone (0.6–0.9 GPa, see O'Reilly et al. 1989). Nepheline, anorthoclase and ulvöspinel would form accessory crystallising phases as the magma fractionated. A further injection of basanitic magma carrying mantle fragments probably broke up the higher level cumulates and intermingled with evolved trachytic melts, which had concentrated K, Ba, S and volatiles before erupting in explosive breccias. Such melt compositions possibly link into syenitic/carbonatitic melts. The age of the explosive emplacement is uncertain on present field relationships. Miocene leucite emplacements are known to occur to the south at Byrock and El Capitan (McQueen 2007) and are inferred to the north east for a volcanic pipe exposed in the Bokhara area (Jaques 2006 and pers. comm. 2007). Buried plugs giving magnetic anomalies are also known to the north east in the Bundabulla area (Madden 1999), where alkali basalt and mantle xenolith-bearing ankaramite were recovered in drill cores recovered below the Early Cretaceous Surat Basin sequence. These bodies suggest Mesozoic to mid-Cenozoic age limits for the Mount Oxley intrusions.

The ultramafic xenoliths in the Mount Oxley intrusives represent mantle lithologies and their thermal conditions at the time of basanite eruption. The spinel meta-harzburgite was re-equilibrated at temperatures between 1000–1035°C, while spinel meta-websterites were re-equilibrated at 985–1000°C, suggesting a slightly higher level origin within an ambient lithospheric geotherm (Figure 8). The absence of garnet in the spinel-bearing metapyroxenites and peridotites favours sampling from above the spinel-garnet pyroxenite and spinel-garnet peridotite transitions respectively (Figure 8). The lack of garnet, however, precludes precise pressure estimates and hence depths of origin, based on garnet-two pyroxene thermobarometry (see Sutherland et al. 2005). Potential pressures can

be assigned from intersections of two-pyroxene re-equilibration temperatures with a known geotherm, but this geotherm dependency produces wide variations from projected models. Several xenolith-derived geotherms proposed for eastern Australian volcanic regions include a Cenozoic South East Australia (SEA) geotherm (O'Reilly and Griffin 1985), a lower temperature variant based on different thermobarometry (Taylor 1998), a more perturbed, higher temperature variant (Sutherland 2003) and an even cooler geotherm (Gaul et al. 2003). Intersections of such geotherms with the Mount Oxley mantle xenolith re-equilibration temperatures are shown in Figure 8. These range in pressure estimate differences by up to 0.5 GPa, or about 15 km in depth for the different models. Using an estimated Moho depth of 38 km (c. 1.05 GPa) for the Bourke-Byrock section (Collins et al. 2003) allows for mantle pressures within the spinel pyroxenite and spinel-peridotite stability fields respectively, compatible with the ultramafic lithological temperatures recorded for the xenolith suite.

Mullagalalah Basalt Petrogenesis

The Mullagalalah basalt fragments are incompletely crystallised, but their main phenocrysts and incipient crystallites suggests they represent a similar but slightly less evolved magma than for the Mount Oxley basanite. The high pressure clinopyroxene and Cr-rich spinel xenocrysts suggest it also incorporated mantle fragments in its evolution. The common amphibole xenocrysts and amphibole-clinopyroxene cumulate assemblages indicate that a hydrous crystallisation was involved at depth, though not necessarily directly from the erupted Mullagalalah magma.

Mount Oxley – Mullagalalah Magmatic Links

The basanitic magmas that produced the Mount Oxley and Mallagalalah intrusions are probably quasi-contemporaneous, but their age relationships to the other Mesozoic-Cenozoic mafic bodies in the area remain untested. They lie along a northern extension of the Miocene

leucite migratory line that trends south from Byrock. If their basanitic magmas formed as part of this trail, although tapping a less potassic mantle source, they would be about 18 Ma in age on extrapolation from the 17.2 Ma age at El Capitan (McQueen et al. 2007). Alternatively, they may be linked to the pre-Early Cretaceous buried alkali basaltic plugs further north at Bundabulla (Madden 1999). The relatively fresh nature of the Mount Oxley and Mullagalalah basanites and their inclusion suites, apart from post-eruptive alteration of the olivines, would suggest Cenozoic links. A fresh appearance, however, is unreliable, as similarly fresh alkali basalts and mantle xenolith suites around Dubbo, NSW, extend from Miocene to Jurassic or older ages (Meakin and Morgan, 1999). The Mount Oxley and Mullagalalah breccia pipes were related to kimberlitic bodies in some exploration reports. The basanitic petrogenesis and lack of obvious garnets within the xenocryst and ultramafic xenoliths, however, weakens such origins and renders the breccias unlikely diamond prospects.

Mount Oxley Features

Distinctive features are nepheline phenocrysts in mantle-origin basanite combined with abundant baryte in hybrid trachyte. The depth of nepheline crystallisation is uncertain, but the mineral can crystallise under mantle conditions (Edgar 1984). Nepheline stability is limited by reactions with SiO_2 in the system, where albite + nepheline gives liquid and nepheline + albite gives jadeite. This gives a maximum stability around 2.4 GPa at 1250°C. Baryte is rather rare in primary magmatic rocks, but is known in late-stage vesicles in porphyritic rhyolite, and in diorite and is common in hydrothermal veins (Zussman 1998). It is also recorded in syenite-carbonatite and lamproite associations (Fitton and Upton 1987) and in lamprophyres (Rock 1991).

Secondary baryte crystals are known in Jurassic alkali basaltic diatremes (Dundas) and alkali dolerite intrusions (Prospect) that intrude the Sydney Basin Triassic beds. At Dundas, baryte is found with calcite and pyrite in vugs in the diatreme and also in veins

within metasedimentary fragments and wall rocks (Australian Museum specimens D35753, D41757). In the Prospect intrusion, baryte is rare and the last mineral to crystallise in the paragenetic sequence (England 1994), where it develops on albite, prehnite, calcite, siderite and pyrite (Australian Museum specimens D35330, D35351, D35686, D38535, D51168, D51170). It would originate from late meteoric hydrothermal fluids, rather than the earlier magmatic deutereric fluids based on oxygen isotope evidence (Williams and Carr 2005). In both the Dundas and Prospect intrusions, baryte was probably derived from barium released from the intruded Triassic shales, whereas the baryte in the Mount Oxley intrusion probably derived from Ba enrichment in fractionated trachytic magma.

ACKNOWLEDGEMENTS

Professor Ian Plimer of the University of Adelaide initiated this study through donations of samples, reports and analytical results in 1983 from the original exploration of the Mount Oxley and Mullagalah intrusions. Ian Matthias, CRA Exploration PL, Cobar, NSW, supplied additional samples and information. Niels Munksgaard, School of Earth Sciences, Macquarie University, facilitated electron microprobe analyses by Jane Barron, while Ken Kinealy, CSIRO Division of Exploration Geoscience, North Ryde, assisted analyses by Lin Sutherland, in 1989. Professor Peter Williams, School of Natural Sciences, University of Western Sydney, facilitated electron microprobe analyses by Adam McKinnon and Lin Sutherland in 2006. Dr Ian Graham, Australian Museum, provided photomicrography of thin sections and Ross Pogson, Australian Museum, assisted through provision of computer programs and mineralogical calculations. Dr Larry Barron, Australian Museum, provided petrological discussion and read the script. Manuscript preparation was aided by Ms Jacqueline Timms, School of Natural Science, University of Western Sydney and Ms Francesca Kelly, St Peters, Sydney. Monique Ferguson kindly helped with the Figures.

The paper is dedicated to Drs Edmund

Potter and Maren Krysko von Tryst for their staunch services to the Royal Society of New South Wales.

REFERENCES

- Byrnes, J.G., 1993. Bourke 1:250 000 Metallogenic Map SH/55-10: Metallgenic Study of Mineral Deposit Data Sheets, 127 pp. Geological Survey of New South Wales, Sydney.
- Cebeira, J.M., 1990. PX: A program for pyroxene classification and calculation. *American Mineralogist* 75, 1426–1427.
- Collins, C.D.N., Drummond, B.J. and Nicoll, M.G., 2003. Crustal thickness patterns on the Australian continent. Evolution and Dynamics of the Australian Plate (Hillis, R.R. and Mueller, R.D., eds), pp. 121–128. *Geological Society of Australia Special Publication* 22 and *Geological Society of America Special Paper* 372.
- Cundari, A., 1973. Petrology of the leucite-bearing lavas in New South Wales. *Journal of the Geological Society of Australia* 20, 465–492.
- Edgar, A.D. 1984. Chemistry, occurrence and paragenesis of feldspathoids: a review. In: *Feldspars and Feldspathoids*, W.L. Brown (ed.) pp. 501–532. D. Reidel Publishing Company, Dordrechet.
- England, B.M., 1994. Minerals of the Prospect intrusion, New South Wales, Australia. *The Mineralogical Record* 25, 185–194.
- Fitton, J.G. and Upton, B.G. J., Eds, 1987. *Alkaline Igneous Rocks*. Geological Society Special Publication No. 30. Oxford, 568 pp.
- Gaul, O.F., O'Reilly, S.Y. and Griffin, W.L., 2003. Lithosphere structure and evolution in Southeastern Australia. Evolution and Dynamics of the Australian Plate (Hillis, R.R. and Mueller, R.D., eds), pp. 185–202. *Geological Society of Australia Special Publication* 22 and *Geological Society of America Special Paper* 372.
- Griffin, W.L., Sutherland, F.L. and Hollis, J.D., 1987. Geothermal profile and crust mantle transition beneath east-central Queensland: volcanology, xenolith petrology and seismic

- data. *Journal of Volcanology and Geothermal Research* 31, 177–203.
- Güven, N., 1988. Smectites. Hydrous Phyllosilicates (exclusive of micas). S.W. Bailey (ed.), pp. 497–559. *Progress in Mineralogy* 19. Mineralogical Society of America.
- Jaques, A.L., 2006. Australian diamond deposits, kimberlites, and related rocks, 1:5 000 000 scale map. Geoscience Australia, Canberra.
- Johnson, R.W. (ed.), 1989. Intraplate Volcanism in Eastern Australia and New Zealand. Cambridge University Press, Cambridge.
- McQueen, K.G., Gonzalez, O.R., Roach, I.C., Pillans, B.J., Dunlap, W.J. and Smith, M.L., 2007. Landscape and regolith features related to Miocene leucitite lava flows, El Capitan northeast of Cobar, New South Wales. *Australian Journal of Earth Sciences* 54, 1–17.
- Madden, J., 1999. EL 5171 Bundabulla First and Final Report Angledool SH 55-07 1:250 000 New South Wales Australia. Geological Survey of New South Wales Report 1999/259.
- Meakin, N.S. and Morgan, E.J., 1999. Dubbo 1:250 000 Geological Sheet SI/55-4 (2nd edition). Geological Survey of New South Wales Explanatory Notes.
- North Broken Hill Ltd, 1971a. Assessment report, EL 292. Bourke-Byrock area. Geological Survey of New South Wales, File GS 1971/346 (unpubl.).
- North Broken Hill Ltd, 1971b. Drilling aid, El 292, Byrock area. Geological Survey of New South Wales, File GS 1971/ 378 (unpubl.).
- North Broken Hill Ltd & Pressaug Australia Pty Ltd 1982. Final report, ELs 1208 and 1209, Mt Oxley, Bourke area. Geological Survey of New South Wales, File GS 1982-339 (unpublished).
- O'Reilly, S.Y. and Griffin, W.L., 1985. A xenolith-derived geotherm for southeastern Australia and its geological implications. *Tectonophysics* 111, 41–63.
- O'Reilly, S.Y., Nicholls, I.A. and Griffin, W., 1989. Xenoliths and megacrysts of Eastern Australia. Intraplate volcanism in Eastern Australia and New Zealand. Johnson, R.W. (ed.), pp. 249–288. Cambridge University Press.
- Paul, B., Herdt, J.M. and Woodhead, J.D., 2005. Mantle heterogeneity beneath the Cenozoic volcanic provinces of central Victoria inferred from trace-element and Sr, Nd, Pb and Hf isotope data. *Australian Journal of Earth Sciences* 52, 243–260.
- Preussag Australia Pty Ltd & North Broken Hill Ltd, 1981a. Exploration reports, 3 and 4, ELs 1208 and 1209, Mount Oxley, Bourke area. Geological Survey of New South Wales, File GS 1981/ 095.
- Preussag Australia Pty Ltd & North Broken Hill Ltd, 1981b. Exploration reports, ELs 1208 and 1209, Mount Oxley, Bourke area. Geological Survey of New South Wales, File GS 1981/ 565.
- Rock, N.M.S., 1991. Lamprophyres. Blackie, Glasgow & London, 285 pp.
- Sutherland, F.L., 1985. Regional controls in eastern Australian volcanism. *Geological Society of Australia, New South Wales Division, Proceedings* 1, 13–32.
- Sutherland, F.L., 2003. Boomerang migratory intraplate Cenozoic volcanism, eastern Australia rift margins and the Indo-Pacific mantle boundary. Evolution and Dynamics of the Australian Plate (Hillis, R.R., and Müller, R.D., eds), pp. 203–221. *Geological Society of Australia Special Publication* 22 and *Geological Society of America Special Paper* 372.
- Sutherland, F.L., Raynor, L.R. and Pogson, R.E., 2005. Table Cape vent xenolith suite, northwest Tasmania: Mineralogy and implications for crust-mantle lithology and Miocene geotherms in Tasmania. *Papers and Proceedings of the Royal Society of Tasmania*, 139, 7–22.
- Sutherland, F.L., Stubbs, D. and Green, D.C., 1977. K-Ar ages of Cainozoic volcanic suites, Bowen-St Laurence hinterland, north Queensland (with some implications for genetic models). *Journal of the Geological Society of Australia* 24, 447–460.
- Tadros, N. (Victor) (Compil. and ed.), 1993. The Gunnedah Basin New South Wales. Ge-

- ological Survey of New South Wales Memoir Geology* 12.
- Taylor, W.R. 1998. An experimental test of some geothermometer and geobarometer formulations for upper mantle peridotites with applications to the thermometry of fertile lherzolite and garnet websterite. *Neues Jahrbuch für Mineralogie, Abhandlungen* 172, 381–408.
- Trebaudino, M. and Bruno, E., 1993. Effects of Al on enstatite solubility in CMAS clinopyroxenes: 1-Experimental results in the clinopyroxene-orthopyroxene two phase field at P=18kbar. *European Journal of Mineralogy* 5, 123–131.
- Wells, P.R.A. (1977). Pyroxene thermometry in simple and complex systems. *Contributions to Mineralogy and Petrology* 62, 129–139.
- Wicks, F.J. and O'Hanly, D.S., 1988. Serpentinite minerals: structures and petrology. Hydrous Phyllosilicates (exclusive of micas), S.W. Bailey, (ed.), pp. 91–167. *Reviews in Mineralogy* 19, Mineralogical Society of America.
- Williams, M.L. and Carr, P.F., 2005. Isotope systematics of secondary minerals from the Prospect intrusion, New South Wales. *Australian Journal of Earth Sciences* 52, 799–806.
- Wood, B.J. and Banno, S., 1973. Garnet orthopyroxene and orthopyroxene-clinopyroxene relationships in simple and complex systems. *Contributions to Mineralogy and Petrology* 42, 109–121.
- Yavuz, F., 1996. Amphcal: A quickbasic program for determining the amphibole name from electron microprobe analysis using the IMA rules. *Computers and Geosciences* 22 (2), 101–107.
- Yoder, H.S., and Tilly, C.E. 1962. Origin of basalt magmas: an experimental study of natural and synthetic rock systems. *Journal of Petrology* 3, 342–532.
- Zhang, M. and O'Reilly, S.Y., 1997. Multiple sources for basaltic rocks from Dubbo, eastern Australia: geochemical evidence for plume-lithosphere mantle interaction. *Chemical Geology* 136, 33–54.
- Zussman, J. 1998. Baryte In Chang L.L.Y, Howie, R.A. and Zussman, J. eds. Rock Forming Minerals. Volume 5B Second Edition. Non-silicates: Sulphates, Carbonates, Phosphates, Halides, pp. 3–29. The Geological Society, London.

* School of Natural Sciences
BCRI Campus, University of Western Sydney
Locked Bag 1797, Penrith South DC
NSW 2197
Australia

† B.J. Barron
7 Fairview Avenue,
St. Ives NSW 2075
Australia

Author for correspondence.
Dr Lin Sutherland
email: L.Sutherland@uws.edu.au

(Manuscript received 27.06.2007, accepted 12.11.2007)